JOURNAL OF MATERIALS SCIENCE **37** (2002) 4307–4313

A deformation processed β-Ti + Y metal–metal composite

P. B. WHEELOCK, K. WONGPREEDEE, A. M. RUSSELL, L. S. CHUMBLEY
Ames Laboratory, Iowa State University, Ames, IA, USA 50011, USA
E-mail: wheelock@ameslab.gov

A Ti-20V-20Y deformation processed metal–metal composite was deformed axisymmetrically by extrusion and swaging to a true strain of 5.9. Tensile strength, ductility, Y phase thickness and spacing, and preferred crystallographic orientation were examined at several levels of true strain as the deformation progressed. The Ti-V metastable BCC solid solution matrix developed a ⟨110⟩ fiber texture. The Y second phase developed a $\langle 10\bar{1}0\rangle$ fiber texture that constrained the Y phase to deform in plane strain. Relatively high tensile ductility was observed at all levels of deformation processing strain.

1. Introduction

1.1. Deformation processed metal–metal composites

During the past quarter century, a new class of composites has been developed with extraordinary mechanical and electrical properties [1–3]. These composites differ from conventional composites in that both the matrix and the reinforcing phase are ductile metals. They can be prepared either by powder metallurgy techniques or by co-melting two metals that are miscible liquids but immiscible solids. The initial P/M or cast billet is heavily deformed, hence the name Deformation-processed Metal Metal Composites (DMMC's). The deformation can be done by extrusion, swaging, drawing, or rolling. Since the phase size reduces in proportion to the reduction in overall billet size, the final microstructure usually consists of phases less than one micrometer thick. Since both metallic phases are ductile, the deformation can be performed to true strain values as high as 16, which corresponds to a 3000-fold reduction in rod diameter.

The metals in a DMMC must either undergo dynamic recovery at the deformation temperature, or they must be annealed periodically to avoid excessive work hardening that could fracture the material. When the deformation becomes extensive, the microstructure typically consists of cylindrical or ribbon-shaped filaments (in wire) or lamellae (in sheet). DMMC's with average second phase thicknesses below 50 nm are common, and some DMMC's have been produced with mean filament or lamellae thicknesses as small as 10 nm.

The nano-scale microstructure of the two metal phases often produces extraordinarily high strengths. An ultimate tensile strength of 4800 MPa has been reported in a Fe-matrix DMMC [4]. Cu-matrix DMMC's have been reported with strengths as high as 2400 MPa [5]. The electrical conductivity of these DMMC's can be quite high also; a wire DMMC is essentially a nano-scale bundle of two pure metals, and conductivities approaching those of the pure metals are common because the electron scattering sites present in solid solution alloys and precipitation hardened alloys are largely absent in DMMC's.

1.2. Ti matrix DMMC's

Copper-BCC transition metal DMMC's (e.g., Cu-20%Nb) are the most thoroughly studied DMMC's. The deformation processing behavior of HCP-HCP Ti-Y DMMC's has been studied previously [6–8] in the hope that a non-cubic deformation processed composite might provide insights into the fundamental mechanism(s) of DMMC strengthening.

In those studies, Ti-50 vol% Y and Ti-20 vol% Y composites were deformation processed to true strains of $\eta = 6.6$ and 7.3 respectively. The smallest filaments produced were about 40 nm thick in the Ti-20Y composite at $\eta = 7.3$, and the ultimate tensile strength of the Ti-20Y increased three-fold from 318 MPa (as-cast) to 945 MPa at $\eta = 7.3$. X-ray texture analysis of the composite specimens showed a strong $\langle 10\bar{1}0\rangle$ fiber texture in both the Ti and Y phases in the deformation processing range $2.2 \leq \eta \leq 7.3$. That texture constrains both the Ti and Y phases to deform by plane strain, which produces severe geometric restrictions on the ability of the plane straining filaments to achieve high η values without fracturing.

1.3. BCC Ti matrix DMMC's

This study examined the mechanical properties and texture of a Ti-20V-20Y DMMC, a BCC Ti-V solid solution matrix containing a pure Y (HCP) second phase. Experience with other DMMC compositions suggested that this BCC matrix plus HCP second phase composite might be expected to form a ⟨110⟩ fiber axis texture in the Ti-V phase and a $\langle 10\bar{1}0\rangle$ fiber axis texture in the Y phase. If the Y phase of the composite had a $\langle 10\bar{1}0\rangle$ fiber axis texture, it would be constrained to deform by plane

strain, because the $\langle 10\bar{1}0\rangle$ fiber axis texture orients the only other active slip system in Y, the $\{0002\}\langle 10\bar{1}0\rangle$, with the slip plane parallel to the tensile axis, resulting in a Schmid factor of zero.

If the BCC matrix had a $\langle 110\rangle$ fiber axis texture, the matrix may also be constrained to deform by plane strain, but the issue is less clear than it is in an HCP Ti matrix. Although no single crystal studies were found in the literature describing the critical resolved shear stress of the slip systems in a Ti-V BCC solid solution, it is reasonable to suppose that the BCC Ti-V solid solution might be able to deform by slip on the $\{211\}\langle 111\rangle$ and/or $\{321\}\langle 111\rangle$ systems as well as the primary $\{110\}\langle 111\rangle$ system. All three of these slip systems contain the same $\langle 111\rangle$ slip direction, but the three slip planes deviate from parallelism with one another by 11° to 41°. Thus, even if the BCC Ti matrix in this composite had a $\langle 110\rangle$ fiber axis texture, the constraint on the matrix to deform by plane strain is less definitive than in the HCP-HCP Ti-20Y DMMC reported previously [6, 8] because of the possibility of cross slip. Whether the final ductility of a BCC Ti matrix would be superior to that of an HCP Ti matrix is difficult to predict *a priori*.

In the Ti-20Y DMMC, it is thought that the texture-imposed plane strain limitation caused the material to break apart when deformation beyond a true strain of 7.3 was attempted. The purpose of this study was to test whether the $\langle 110\rangle$ and $\langle 10\bar{1}0\rangle$ fiber axis textures form in a BCC-Ti plus HCP-Y composite, and if so, whether the material would suffer the same inability to tolerate high deformation true strains. The condition of plane strain does not necessarily limit the ability of a BCC material to tolerate large deformation processing true strains. High purity Nb, for example, develops the $\langle 110\rangle$ fiber texture, but it will tolerate extraordinarily large deformations by wire drawing [9] without fracture. Thus, even if the BCC matrix of the Ti-20V-20Y DMMC assumed a $\langle 110\rangle$ fiber texture, it might still tolerate very large deformation processing true strains such as those seen for the Cu-Nb and other FCC matrix DMMC's. The smaller phase thickness and spacing that greater amounts of deformation processing could produce in such a high η Ti specimen might allow it to achieve exceptionally high levels of tensile strength, offering a relatively simple method to achieve ultra-high strength in Ti.

2. Experimental procedures

2.1. Alloy preparation and deformation

In this study a DMMC of 60 weight% Ti, 20 weight% V, and 20 weight% Y was produced. Y and Ti are mutually immiscible in the solid state, so this alloy solidifies with a matrix phase of β-Ti (a metastable BCC solid solution of 75%Ti and 25%V) with an Y second phase. The material for this experiment was prepared by arc melting pure Ti, V, and Y to form fingers and combining these to form an electrode for a mini-consumable melt. The electrodes were melted consumably into a 31.8 mm diameter mold. Although the binary equilibrium phase diagram for Ti-V predicts a two-phase HCP-Ti + BCC-V structure for a 75Ti-25V alloy below 950 K, the transformation to the equilibrium two-phase structure during cooling is sluggish. X-ray diffraction of the material at room temperature showed the matrix to be a metastable single-phase BCC Ti-V solid solution; no HCP α-Ti XRD peaks were detected in the as-cast or the deformation processed material.

After casting, the ingot was machined to 26 mm diameter to produce a uniform cylinder free of surface voids. The machined ingot was inserted into a steel can, and this can was inserted into a thin-walled copper can of 51 mm outside diameter and sealed. This assembly was heated to 1150 K and extruded through a 13.5 mm die. This extruded 13.5 mm rod was the starting material for the experiment.

The 13.5 mm diameter specimen, still jacketed in steel and Cu from the extrusion can, was heated in a 950 K muffle furnace long enough to reach the furnace temperature; time at 950 K was kept to a minimum to reduce the possibility of spheroidization and coarsening of the Y phase. This was done by comparing the color of the sample to the color of the furnace walls and removing the specimen for the next swaging operation as soon as the colors matched. The sample was swaged through a sequence of dies as follows: 10.8 mm, 9.1 mm, 7.7 mm, 6.9 mm, and 6.1 mm. From this point, the material was deformed further using a cold-work/anneal cycle. Each cold work cycle was done by swaging through two successively smaller swaging dies, each of which reduced the specimen diameter by approximately 8%. The anneal for each cycle was performed in a vacuum furnace at 900 K for 1.8 ks. Five cold-work and anneal cycles were performed to reduce the specimen diameter to 2.9 mm. Finally, the specimens were cold swaged through two additional dies without any annealing to a final diameter of 2.5 mm. Although the specimens were still ductile even at the smallest diameter, no further cold work was attempted , due to the difficulty of performing tensile tests on such small diameter rod.

2.2. Tensile testing procedures and ductility measurements

Tensile testing was performed on specimens taken from the material at various levels of deformation processing true strain (η), where true strain is calculated as $\eta = \ln(\text{area}_{\text{original}}/\text{area}_{\text{final}})$. Two tensile test specimens were pulled for each η value reported, and the average of the two values is reported in the table and figure.

Tensile test specimens were pulled at a crosshead speed of 4.2 μm/s. For all tensile tests, a value of engineering ultimate tensile strength was calculated from the quotient of the applied maximum load and the initial cross sectional area of the specimen. Ductility was calculated for each specimen by measuring the area of the fracture surface in a traveling microscope and comparing that area to the original cross sectional area of the specimen to calculate the percent reduction in area.

2.3. Specimen preparation for SEM examination and orientation imaging microscopy texture analysis

Scanning electron microscopy (SEM) specimens were prepared by ordinary metallographic techniques and

examined in an unetched condition. The large disparity in atomic number between the Ti-V solid solution and Y provided strong contrast when using back-scattered electron imaging. Phase thickness determinations were made from the SEM photographs by measuring phase thicknesses across their short dimension and averaging these values. Phase spacing determinations were made from the SEM photographs by normal stereology methods [10].

Texture analysis was performed by X-ray diffraction and by orientation imaging microscopy (OIM) analysis with a scanning electron microscope (SEM) on material deformation processed to $\eta = 2.6$. The OIM specimen was cleared of oxide layers by a brief ion beam bombardment immediately prior to examination; the OIM experimental methods have been described in detail elsewhere [6]. Later OIM examination of the same specimen was performed after a 1.8 ks stress relief anneal at 900 K.

3. Results

3.1. The effect of deformation on microstructure

As expected, the Ti-20V-20Y composite displayed progressively finer Y phase thickness and spacing with increasing amounts of deformation. The as-cast microstructure was characteristic of two immiscible metals with the Ti-V solid solution forming the matrix and Y dendrites forming the second phase (Fig. 1). Initial hot work changed the original dendritic structure to a filamentary structure; Figs 2 and 3 show the microstructure at $\eta = 2.6$ and $\eta = 5.9$. The phase size measurements taken from the SEM micrographs are shown in Table I.

As Fig. 1 shows, the as-cast microstructure had Y phase thicknesses that ranged from about 1–20 μm; a few Y phase thicknesses as large as 60–100 μm were observed in some locations in the as-cast sample. This wide variation in Y phase thickness was largely eliminated by the hot extrusion which was used to begin the deformation processing. It is thought that the flow stress of the high-purity Y phase at the 1150 K extrusion temperature was much lower than the flow stress of the BCC Ti-V solid solution matrix, causing the Y to deform more than the matrix and preferentially thinning the Y phases that had been largest in the as-cast material. A typical microstructure of the as-extruded material is shown in Fig. 2; no Y filaments with thickness greater than 8–10 μm were observed in these two micrographs or in any of the several others taken of the as-extruded material. The transverse section of the as-extruded material shows the convoluted ribbon shape characteristic of a second phase constrained to plane strain deformation. This same convoluted ribbon morphology was evident in the Y phase at all deformation levels from $\eta = 2.6$–5.9 (Figs 2 and 3).

At the highest deformation levels attained ($\eta = 5.9$), the Y filaments were reduced to an average thickness of only 130 nm. Although such a filament thickness is relatively small, it falls well short of the 10 to 30 nm mean filament thickness seen in the Cu-Nb DMMC's that displayed the highest tensile strengths. The relatively small initial size of the Ti-20V-20Y specimen in

TABLE I Average phase sizes measured by SEM for Ti-20V-20Y

True strain of deformation processing (η)	Average Y filament thickness (μm)	Y filament thickness standard deviation (μm)	Average Y filament spacing (μm)	Specimen condition
2.6	0.59	0.138	2.28	As-extruded at 1150 K
3.5	0.27	0.050	0.90	As-swaged at 900 K
5.5	0.14	0.033	0.52	Cold swaged
5.9	0.13	0.048	0.47	Cold swaged

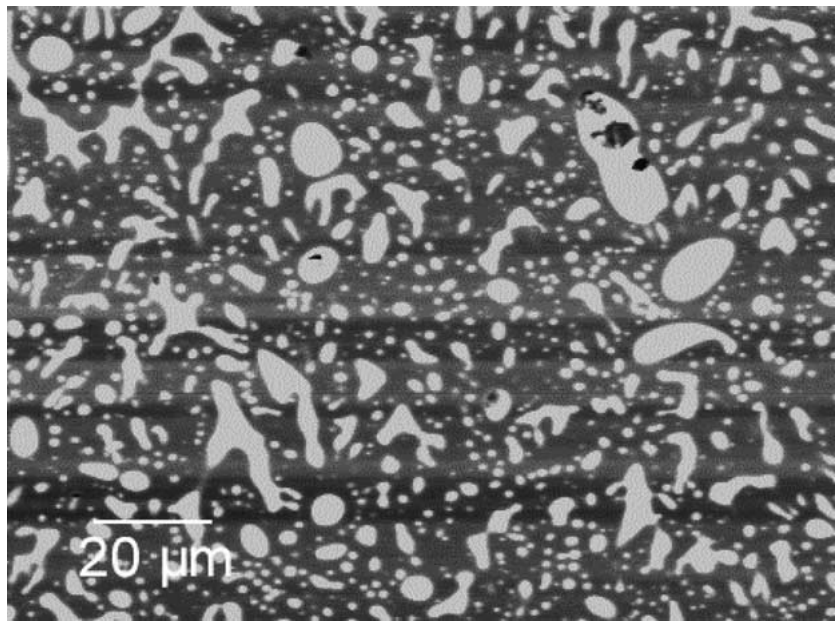

Figure 1 SEM back-scattered electron micrograph of the microstructure of as-cast Ti-20V-20Y ($\eta = 0$). The dark phase is Ti-V solid solution; the light phase is Y. Note the large variation in Y phase thicknesses, ranging from about 1–20 μm.

this study would have made it difficult to achieve the very high deformation levels ($\eta = 10$–12) at which the highest strengths were observed in Cu-Nb. This specimen would have to be reduced to a diameter of only 92 μm to achieve a deformation processing true strain of 12.

3.2. The effect of deformation on mechanical properties

As would be expected, deformation processing substantially increased the ultimate tensile strength (UTS) of the Ti-20V-20Y composite. Ultimate tensile strength and ductility data from the tensile testing are presented in Table II and in Fig. 4.

Fig. 4 shows that the composite nearly doubled in UTS as η increased from 0 to 5.9, similar to the UTS increase seen in Cu-20Nb and in the Ti-20Y composite studied earlier [5, 6] for similar η values. The as-cast ultimate tensile strength is more than double the ultimate tensile strength of as-cast Ti-20%Y specimens measured in previous studies [6] due to the solid solution hardening effect of the V in the Ti matrix. The maximum strength is seen at the highest deformation level where the kinked ribbon-shaped phases were thinnest and most closely spaced in the matrix; this behavior is typical of DMMC's.

TABLE II Tensile test data for Ti-20V-20Y

True strain of deformation processing (η)	Ductility (% area reduction	Ultimate tensile strength (MPa)	Specimen condition
0	NA	536	As-cast
2.6	42	635	As-extruded at 1150 K
3.5	48	676	As-swaged at 900 K
5.5	58	850	Cold swaged
5.9	55	896	Cold swaged

3.3. Texture measurements

The first texture analysis for these specimens was done by a simple comparison of XRD peak intensities from

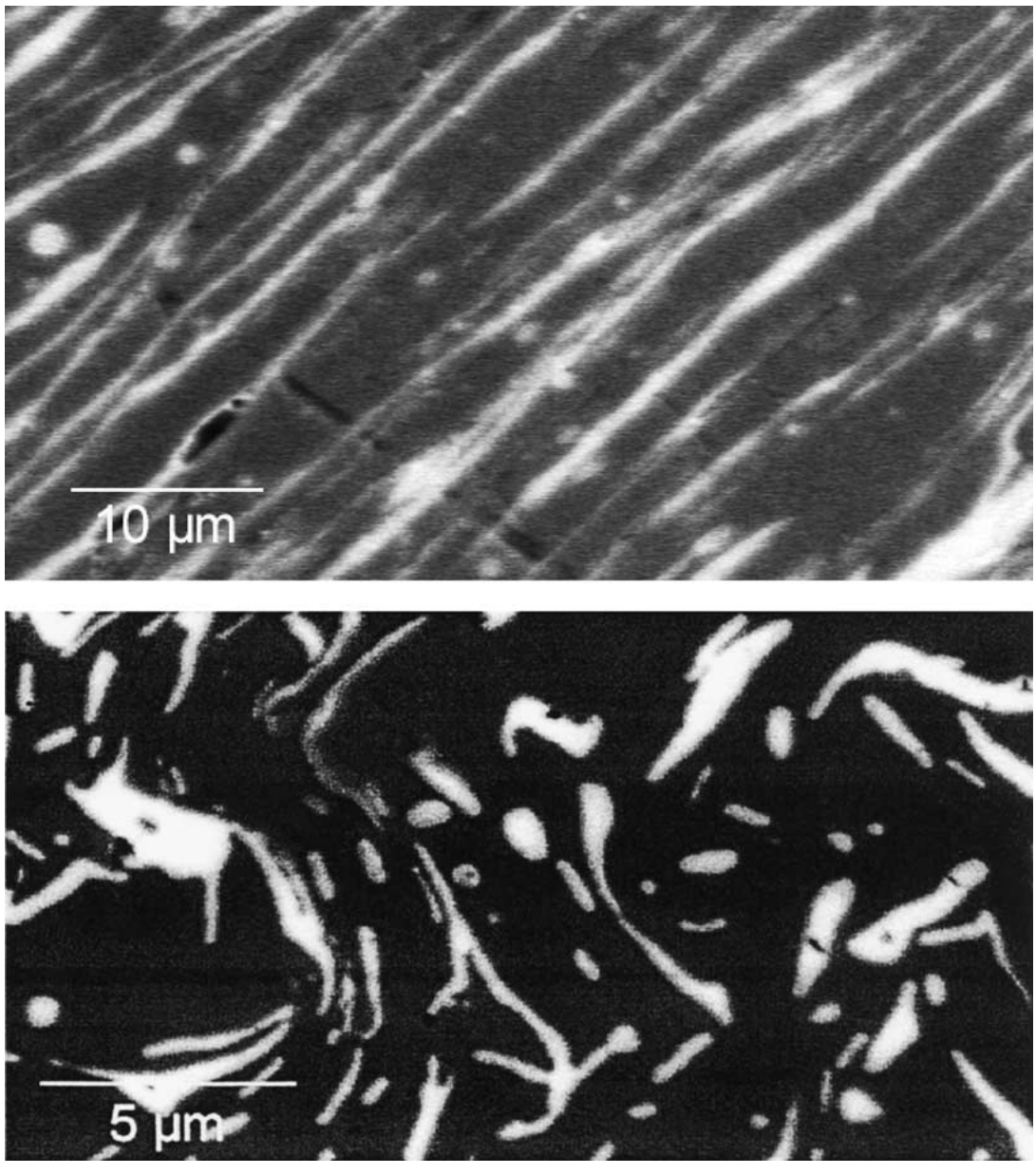

Figure 2 SEM back-scattered electron micrographs of a longitudinal section (upper image) and a transverse section (lower image) of the filamentary microstructure in Ti-20V-20Y extruded at 1150 K to $\eta = 2.6$. Dark gray areas are Ti-V solid solution; light gray areas are Y. Note that the Y phase size shows much less variability than was observed in the as-cast material in Fig. 1.

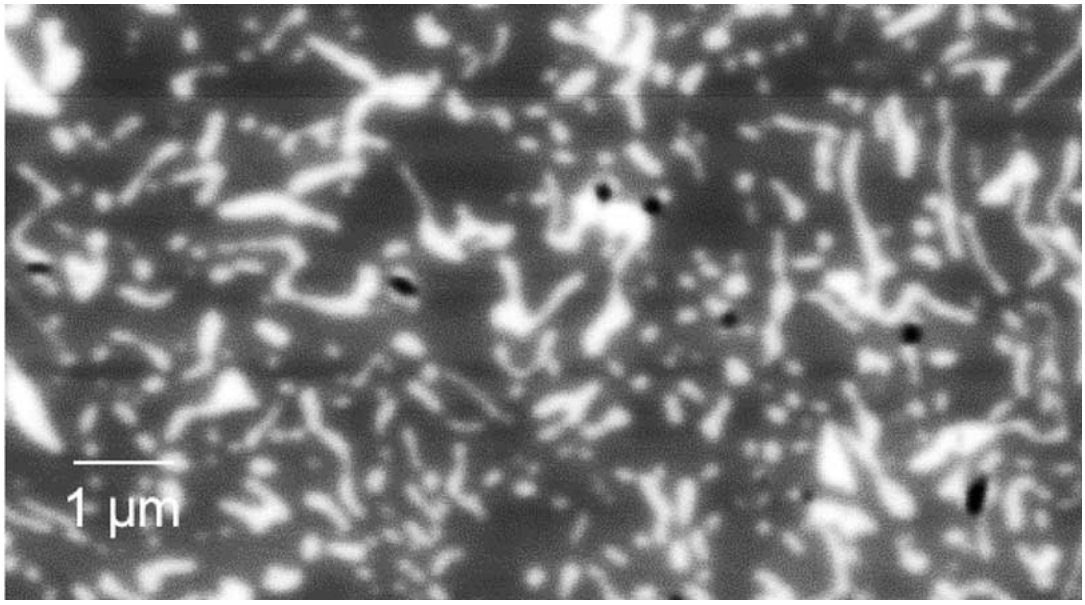

Figure 3 SEM back-scattered electron micrograph of a transverse section of filamentary microstructure in Ti-20V-20Y deformation processed to $\eta = 5.9$. Dark gray areas are Ti-V solid solution; light gray areas are Y.

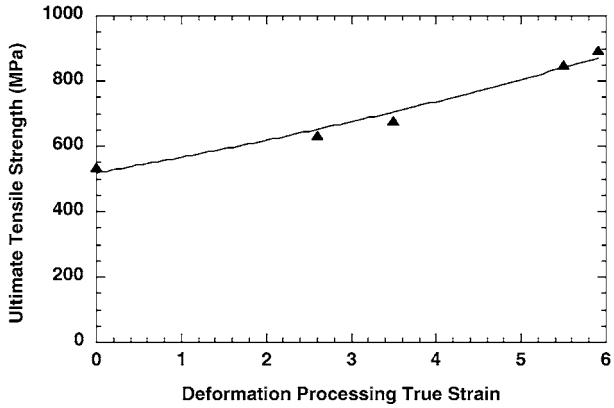

Figure 4 Ultimate tensile strength of Ti-20V-20Y plotted against deformation processing true strain.

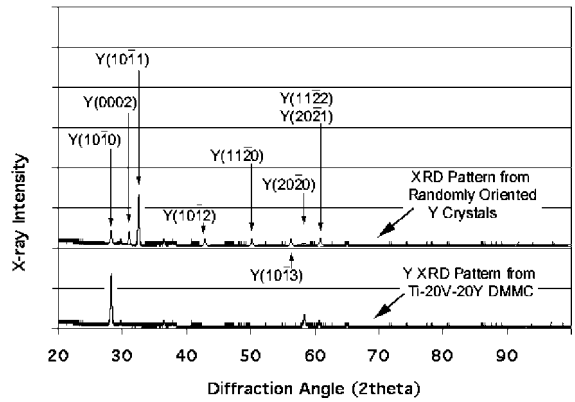

Figure 5 X-ray diffraction patterns from a reference sample of randomly oriented Y grains [11] (upper curve) and the heavily textured Y filaments in the Ti-20V-20Y DMMC of this study (lower curve). The peaks from the BCC Ti-V matrix phase have been removed for clarity. Note that, due to the strong $\langle 10\bar{1}0 \rangle$ fiber texture in the DMMC, only the (1010) and the (2020) Y peaks have any discernible intensity on the lower curve.

randomly oriented grains of Ti-V solid solution and pure Y with the peak intensities obtained by XRD θ-2θ scans on the DMMC specimens at various η values. This approach showed that the HCP Y second phase had a strong $\langle 10\bar{1}0 \rangle$ fiber texture, and the BCC matrix had a strong $\langle 110 \rangle$ fiber texture (Figs 5 and 6). This result is not surprising, since a $\langle 110 \rangle$ fiber texture is normally observed in drawn BCC metals [9], and occurrence of a $\langle 10\bar{1}0 \rangle$ fiber texture was also observed in the Y phase of the Ti-20Y DMMC in earlier studies [6, 8]. Although XRD θ-2θ scans of this type can indicate the presence of texture, they do not give accurate quantitative information about the degree of preferred orientation; for that, OIM analysis was performed on one of the Ti-20V-20Y specimens.

The initial OIM analysis of a transverse section of the as-extruded material produced texture determinations with unacceptably low confidence factors (~25%) and showed no reproducible texture determinations from one scan to the next. Since residual stresses in the specimen can degrade the quality of OIM data, the specimen was then given a 1.8 ks stress relief anneal at 900 K. Prior work with Ti DMMC's had shown that recrystallization does not occur below 1000 K for this time

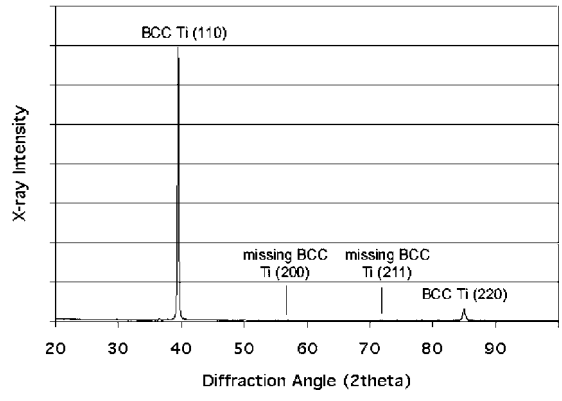

Figure 6 X-ray diffraction pattern from the BCC Ti-V matrix phase in the Ti-20V-20Y DMMC of this study. The Y peaks have been removed for clarity. Note that only two Ti-V solid solution peaks, the (110) and the (220), have any discernible intensity on the lower curve. Due to the presence of a strong $\langle 110 \rangle$ fiber texture in this phase, the (200) and the (211) peaks are both completely absent, even though they would be two to three times stronger than the (220) peak in a Ti-V BCC solid solution with randomly oriented grains.

interval in HCP Ti, so this anneal was intended to provide stress relief without recrystallizing the material. After annealing, OIM analysis of the specimen showed isolated regions a few micrometers across with a strong (∼12 times random) ⟨111⟩ fiber texture, but all other areas displayed the same low confidence factors that had been observed prior to the anneal.

These contradictory results from XRD θ-2θ scans and OIM are probably attributable to the difference in the sample volume scanned by the two methods. For XRD using Cu X-rays incident on a Ti sample, the diffracted signal emanates from a depth of 0–20 μm below the sample surface; however, the back-scattered electrons used for OIM analysis emanate from a depth of only 0–0.2 μm. The very thin specimen volume probed by OIM 0.1 or 0.2 μm below the surface carries residual stresses from metallographic polishing and may experience recrystallization at anomalously low temperatures due to the presence of the free surface. The much deeper specimen volume probed by XRD is presumably more representative of the total specimen volume. For this reason the XRD texture determination was used in analyzing the material in this study.

4. Discussion

4.1. Texture induced plane strain in both matrix and second phase

In the Cu-X deformation processed composites (where X is a BCC transition metal second phase insoluble in Cu), the second phase typically forms a ⟨110⟩ fiber texture while the Cu matrix develops a ⟨111⟩ fiber texture often accompanied by a ⟨001⟩ fiber texture [1, 12–15]. Fig. 7 shows a BCC crystal with a ⟨110⟩ fiber texture. This texture positions two of the four ⟨111⟩ directions (the $[1\bar{1}1]$ and the $[\bar{1}\bar{1}1]$) perpendicular to the center line, which makes slip impossible. All slip is limited to the remaining two ⟨111⟩ directions (the [111] and the $[\bar{1}11]$) which lie opposite one another across the specimen center line, thus limiting the BCC phase to plane strain [1, 9]. The FCC Cu matrix, however, can readily deform axisymmetrically in either the ⟨111⟩ or ⟨001⟩ fiber texture, since these orientations possess three and four slip directions respectively to accommodate plastic flow. The Cu-X deformation processed composites are therefore characterized by plane straining BCC second phases embedded in a Cu matrix whose several active slip systems can accommodate the changing filament aspect ratios of the second phase.

In the Ti-20Y deformation processed composites studied previously [7], the observed $\langle 10\bar{1}0\rangle$ fiber texture in the Y limits the Y second phase to plane strain in the same manner as the BCC second phase in the Cu-X DMMC's was limited to plane strain. This results from the orientation of the two slip systems thought to be active in Y at room temperature, the (0002) $\langle 11\bar{2}0\rangle$ and the $\{10\bar{1}0\}$ $\langle 11\bar{2}0\rangle$. In an HCP metal with a $\langle 10\bar{1}0\rangle$ fiber texture, the (0002) $\langle 11\bar{2}0\rangle$ slip system has a resolved shear stress of zero, and thus would be incapable of contributing to plastic flow. If Schmid's Law is applied to the $\{10\bar{1}0\}$ $\langle 11\bar{2}0\rangle$slip system in a rod with the $\langle 10\bar{1}0\rangle$ fiber texture, λ becomes 30° and ϕ becomes 60°, which yields a resolved shear stress of:

$$\tau_r = \sigma \cos\phi \cos\lambda = \sigma \cos(60^\circ)\cos(30^\circ) = 0.433\sigma$$

A resolved shear stress of 0.433σ is near the maximum possible value of 0.5σ, and this slip system must be the active one in axisymmetrically deformed HCP specimens with the $\langle 10\bar{1}0\rangle$ fiber texture. However, the orientation of the $\{10\bar{1}0\}$ $\langle 11\bar{2}0\rangle$slip system in material with a $\langle 10\bar{1}0\rangle$fiber texture permits only plane strain deformation, as shown in Fig. 8. Thus, the ribbon-shaped

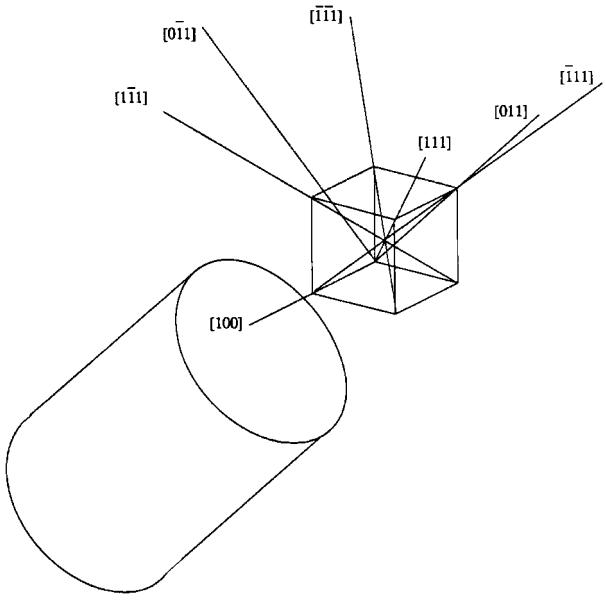

Figure 7 In a BCC crystal with a ⟨110⟩ fiber texture, two of the four ⟨111⟩ directions (the $[1\bar{1}1]$ and $[\bar{1}\bar{1}1]$ the) are positioned perpendicular to the center line and thus cannot slip. All slip on {110} planes is limited to the remaining two ⟨111⟩ directions, the [111] and the $[\bar{1}11]$, which lie opposite one another across the specimen center line [1, 10].

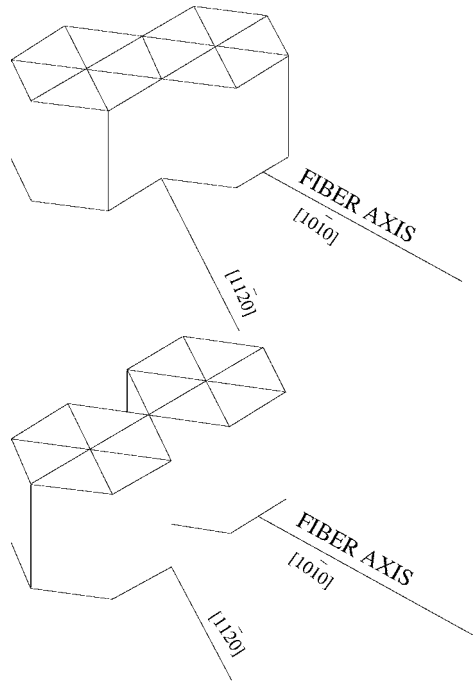

Figure 8 Illustration of the relative orientations of six hexagonal close-packed unit cells with a $\langle 10\bar{1}0\rangle$ fiber texture before and after a slip of one Burger's vector magnitude on the $\{10\bar{1}0\}$ $\langle 11\bar{2}0\rangle$ slip system. Since this is the only active slip system in Y with a $\langle 10\bar{1}0\rangle$ fiber texture, the metal is constrained to plane strain deformation.

Y filaments seen in Figs 2 and 3 are the shape expected for a plane straining phase, and the Y filaments are similar to the plane straining BCC second phases seen in the well-studied Cu-X DMMC's.

4.2. The potential ability of Ti-20V-20Y to tolerate large deformation strains

If slip is limited to the {110} planes in BCC Ti, the BCC matrix phase in the Ti-V-Y composite is also constrained to deform by plane strain because it has the ⟨110⟩ fiber texture. In that case both the Ti-V matrix and the Y second phase would be limited to plane strain by their textures, the twisted ribbon shape seen in the BCC filaments of Cu-X composites would be expected for both phases in the Ti-V-Y composite. The very thin filaments with exceptionally large interfacial boundary area inherent in a DMMC where both phases deform by plane strain might be expected to produce the anomalous strengthening observed with the FCC/BCC Cu-X composites but absent in the FCC/FCC composites such as Ag-Cu. [16]. Indeed, the increase in strength observed for this Ti-20V-20Y composite in Fig. 4 is similar to that observed in the Cu-20Nb composites [1–3] over an equivalent range of η values. However, the ⟨110⟩ fiber texture of the Ti-V BCC matrix does not limit strain to plane strain, since the possibility exists for other BCC slip systems such as the {211} ⟨111⟩ and/or {321} ⟨111⟩ to slip. As noted previously, all three of these slip systems have the ⟨111⟩ slip direction, but these three slip planes deviate from parallelism with one another by 11° to 41°. Thus, the ⟨110⟩ fiber axis texture in the BCC Ti matrix does not enforce plane strain as rigorously as does the $\langle 10\bar{1}0\rangle$ fiber texture in HCP Y and Ti. The fact that the Ti-20V-20Y tolerated deformation to $\eta = 5.9$ is an encouraging indication for the ability of this composite to achieve higher η levels, but the result is not conclusive.

During the various deformation processing operations performed on the earlierTi-20Y and Ti-50Y composites, those composites showed decreasing tensile test ductility as the deformation processing true strain increased, and they eventually became so brittle that further deformation was impossible. None of these specimens was ever deformed to a total true strain greater than 7.3 without breaking. As described elsewhere [6–8], this inability to tolerate large true strains is thought to result from the geometrical impossibility of deforming a composite in which both of the phases present are deforming by plane strain.

The decrease in tensile test ductility that has been observed in previous studies of Ti-20Y [6, 8] is notably absent in this Ti-20V-20Y DMMC. As Table II indicates, the composite with the highest deformation processing true strain ($\eta = 5.9$) still displayed 55% reduction in area ductility during tensile testing. It may be that one or more of the other slip systems that are commonly active in BCC metals (the {211} ⟨111⟩ and the {321} ⟨111⟩) are active in the BCC Ti-V matrix phase, avoiding the loss of ductility seen in the HCP-HCP Ti-Y DMMC's studied earlier.

This study did not reach high levels of deformation processing since the initial billet was small. The fact that the ductility of the composite was still high at the final deformation level of $\eta = 5.9$, raises the intriguing possibility that the Ti-20V-20Y DMMC may be capable of reaching very high deformation processing true strains without experiencing the brittleness problems that terminated deformation processing in the Ti-Y DMMC's. If this is indeed the case, it may also be possible to achieve the high ultimate tensile strengths that typically accompany the finest second phase thicknesses and spacings. The finest average Y phase spacing seen in this study was 130 nm. In Cu-20Nb DMMC's, the ultimate tensile strength at very high levels of deformation processing ($\eta \geq 12$) reached values as high as 2200 MPa when the Nb filament thickness averaged 10–30 nm.

Acknowledgements

The authors are grateful to L. L. Jones, F. C. Laabs, J. T. Wheelock, L. P. Lincoln, L. Hood, and L. K. Reed, all of Ames Laboratory for their valuable discussions and for preparing and characterizing the materials used in this study. This work was performed at Ames Laboratory, operated for the U.S. Department of Energy by Iowa State University under contract number W-7405-ENG-82.

References

1. A. RUSSELL, L. CHUMBLEY and Y. TIAN, *Adv. Engr. Mater*. **2** (2000) 11.
2. J. VERHOEVEN, F. SCHMIDT, E. GIBSON and W. SPITZIG, *J. Metals* **38**(9) (1986) 20.
3. M. MORRIS and D. MORRIS, *Matls. Sci. and Eng. A* **111** (1989) 115.
4. J. EMBURY and R. FISHER, *Acta Metall.* **14** (1966) 147.
5. J. BEVK, J. HARBISON and J. BELL, *J. Appl. Phys.* **49**(12) (1978) 6031.
6. A. RUSSELL, L. CHUMBLEY, F. LAABS and J. RUSSELL, *J. Mater. Sci.* **34** (1999) 1447.
7. A. RUSSELL, L. CHUMBLEY, T. ELLIS, F. LAABS, B. NORRIS and G. DONIZETTI, *ibid.* **30** (1995) 4249.
8. A. RUSSELL, T. ELLIS and L. CHUMBLEY, *ibid.* **30** (1995) 2070.
9. W. HOSFORD, JR., *Trans. Met. Soc. AIME* **230** (1964) 12.
10. E. UNDERWOOD, in "Quantitative Stereology" (Addison-Wesley, 1970) Ch. 3–4.
11. Natl. Bur. Stand. (U.S.) Monograph **25**(18) (1981) 77.
12. A. PELTON, F. LAABS, W. SPITZIG and C. CHENG, *Ultramicroscopy* **22** (1987) 251.
13. J. VERHOEVEN, W. SPITZIG, L. JONES, H. DOWNING, C. TRYBUS, E. GIBSON, L. CHUMBLEY, L. FRITZMEIER and G. SCHNITTGRUND, *J. Matls. Eng.* **12**(2) (1990) 127.
14. C. TRYBUS, Ph.D. Dissertation, Iowa State University (1988).
15. M. MORRIS and D. MORRIS, *Acta Metall. Mater.* **39**(8) (1991) 1763.
16. G. FROMMEYER and G. WASSERMANN, *Acta Metall.* **23** (1975) 1353.

Received 5 February
and accepted 2 July 2002